The Non-Gaussian Nature of Prostate Motion Based on Real-Time Intrafraction Tracking

Yuting Lin, *University of California, Irvine*
Tian Liu, *Emory University*
Wells Yang, *Georgia Institute of Technology*
Xiaofeng Yang, *Emory University*
Mohammad Khan, *Emory University*

Journal Title: International Journal of Radiation Oncology - Biology - Physics
Volume: Volume 87, Number 2
Publisher: Elsevier | 2013-10-01, Pages 363-369
Type of Work: Article | Post-print: After Peer Review
Publisher DOI: 10.1016/j.ijrobp.2013.05.019
Permanent URL: https://pid.emory.edu/ark:/25593/rk4d0

Final published version: http://dx.doi.org/10.1016/j.ijrobp.2013.05.019

Copyright information:

Published in final edited form as:

Int J Radiat Oncol Biol Phys. 2013 October 1; 87(2): 363–369. doi:10.1016/j.ijrobp.2013.05.019.

The Non-Gaussian Nature of Prostate Motion Based on Real-Time Intrafraction Tracking

Yuting Lin, PhD[*], **Tian Liu, PhD**[†], **Wells Yang**[‡], **Xiaofeng Yang, PhD**[†], and **Mohammad K. Khan, MD, PhD**[†]

[*]Tu and Yuen Center for Functional Onco-Imaging, Department of Radiological Sciences, University of California, Irvine, California

[†]Department of Radiation Oncology Emory University Hospital, Winship Cancer Institute, Atlanta, Georgia

[‡]Department of Biomedical Engineering, Georgia Institute of Technology, Atlanta, Georgia

Abstract

Purpose—The objective of this work is to test the validity of the Gaussian approximation for prostate motion through characterization of its spatial distribution.

Methods and Materials—Real-time intrafraction prostate motion was observed using Calypso 4-dimensional (4D) nonradioactive electromagnetic tracking system. We report the results from a total of 1024 fractions from 31 prostate cancer patients. First, the correlation of prostate motion in right/left (RL), anteroposterior (AP), and superoinferior (SI) direction were determined using Pearson's correlation of coefficient. Then the spatial distribution of prostate motion was analyzed for individual fraction, individual patient including all fractions, and all patients including all fractions. The displacement in RL, AP, SI, oblique, or total direction is fitted into a Gaussian distribution, and a Lilliefors test was used to evaluate the validity of the hypothesis that the displacement is normally distributed.

Results—There is high correlation in AP/SI direction (61% of fractions with medium or strong correlation). This is consistent with the longitudinal oblique motion of the prostate, and likely the effect from respiration on an organ confined within the genitourinary diaphragm with the rectum sitting posteriorly and bladder sitting superiorly. In all directions, the non-Gaussian distribution is more common for individual fraction, individual patient including all fractions, and all patients including all fractions. The spatial distribution of prostate motion shows an elongated shape in oblique direction, indicating a higher range of motion in the AP and SI directions.

Conclusions—Our results showed that the prostate motion is highly correlated in AP and SI direction, indicating an oblique motion preference. In addition, the spatial distribution of prostate motion is elongated in an oblique direction, indicating that the organ motion dosimetric modeling

Reprint requests to: Mohammad K. Khan, MD, PhD, 1365 Clifton Road NE, Department of Radiation Oncology, Emory University Hospital, Winship Cancer Institute, 1365 Clifton Rd NE, Atlanta, GA 30345. Tel: (404) 778-4126; drkhurram2000@gmail.com.

Conflict of Interest: none.

Supplementary material for this article can be found at www.redjournal.org.

using Gaussian kernel may need to be modified to account for the particular organ motion character of prostate.

Introduction

During prostate cancer external beam radiation therapy, the knowledge of organ motion is essential to ensure conformed dose delivery to the target while minimizing toxicity to the surrounding organs at risk. Organ motion leads to smearing of dose distribution, causing reduced sharpness of intended dose conformality (1, 2). Interfraction motion will not cause blurring in a given fraction; rather, the total accumulated dose distribution will be blurred. To characterize and minimize the interfraction motion, various daily localization techniques have been developed, such as surface fiducial or 3-point surface alignment, implanted fiducial, or bony landmark with on board imaging, ultrasound, and kV/mV CBCT (3–5). Meanwhile, the daily intrafraction motion also plays an essential role in determining treatment planning margin (6), and may be a function of how frequent the prostate motion is sampled during a course of treatment (7).

Decreasing the planning target volume (PTV) margins can potentially reduce the radiation exposure to normal tissue and limit the toxicity and side effect for treatment. To decrease PTV margins in a safe manner, precise understanding and proper modeling of the intrafraction motion is critical. High precision, real-time intrafraction prostate motion was obtained using Calypso 4D nonradioactive electromagnetic tracking system. Three electromagnetic transponders (“Beacon”) were implanted into the prostate. During daily radiation treatments, the Beacon transponders communicated with the Calypso System through nonionizing radiofrequency signal and the prostate isocenter displacement in SI, AP, and lateral directions is recorded at a 10-Hz frequency. The availability of these measurements allows us to evaluate and characterize the intrafraction prostate motion in detail—in particular, whether or not the motion errors can be represented by a Gaussian function.

The objectives of this work were: (1) to investigate the directional dependence and correlation of prostate motion; and (2) to characterize and quantify the spatial distribution of the prostate motion.

Methods and Materials

Patient and calypso implantation procedure

A total of 31 patients were included in this study. These subjects were clinically diagnosed with prostate cancer and treated with intensity modulated radiation therapy at the Taussig Cancer Institute at Cleveland Clinic. Three Beacon electromagnetic transponders were implanted into the prostate via transrectal ultrasound guidance before the radiation treatment. Intrafractional motion of the prostate is monitored at 10-Hz frequency of the RL, AP, and SI displacement of the isocenter using the Calypso 4-dimensional (4D) tracking system. Our Calypso technique, which was instrumental in initial US Food and Drug Administration approval for the Calypso system, has been previously described (8, 9). Briefly, all patients were treated in the supine position with a band placed around the feet, a

wedge under the knees, a ring for the hands on the chest, and a Vac-Loc bag for daily immobilization purposes. They were instructed to drink 500 mL of fluid 4 hours before the daily treatments. A low-residue diet was encouraged during treatments and patients were encouraged to have a bowel movement earlier during the day before treatments. Typical intensity modulated radiation therapy treatments included 38–39 daily fractions, and only the fractions consisting of a minimum of 3 minutes' continuous tracking data are included in the analysis, resulting in a total of 1024 fractions.

Prostate motion direction correlation

To characterize the directional dependency of prostate motion, the correlation in RL, AP, and SI direction from tracking data were determined using Pearson's correlation of coefficient. The magnitude of correlation coefficient ≥0.7 indicates a strong correlation between 2 directions. Medium correlation is defined by the magnitude of correlation coefficient between 0.5 and 0.7. The magnitude of correlation coefficient between 0.3 and 0.5 indicates a low correlation, and little if any correlation exists for those data pairs whose magnitude of coefficient is <0.3. A 99% confidence interval for the correlation coefficient is required.

Prostate motion distribution analysis: individual fraction

The procedure to account for motion and setup error in dose calculation uses Gaussian approximation to describe the blurring effect. Because it has been long believed that prostate motion and setup errors are random, Gaussian approximation is considered to be good without loss of generality, especially after multiple fractions based on the central limit theorem (2, 10). To evaluate the validity of the Gaussian approximation assumption, the prostate motion was characterized using real-time tracking data during radiation treatment.

For each fraction of each patient, the tracking data indicating displacement in RL (x axis) direction, AP (y axis) direction, and SI (z axis) direction was obtained. The total displacement in the oblique direction ($\sqrt{y^2+z^2}$) and the total displacement in all directions ($\sqrt{x^2+y^2+z^2}$) were also calculated. Afterward, the displacement was fitted into a Gaussian distribution and was used to evaluate the validity of the hypothesis that the distribution is normally distributed. The Lilliefors test was used when the null distribution is unknown and has to be estimated (11). This was suitable for our study because we were interested in whether or not the distribution is Gaussian with any mean and variance.

Prostate motion distribution measurement: total fractions of one patient

We evaluated the validity of the Gaussian approximation assumption of accumulative fractions of prostate motion from a single patient. Only those patients who had more than 30 valid fractions were included in this analysis, resulting in 24 patients in total. All the fractions of displacement tracking data were combined into a single array, and displacement in RL, AP, SI, oblique, and all directions were calculated for each patient. The same Gaussian distribution test was used to quantify the displacement on an individual patient level.

Prostate motion distribution measurement: total fractions from all patients

Last, we evaluated the validity of Gaussian approximation assumption of accumulative fractions of prostate motion from all patients on a population level. The recorded displacements from all 24 patients who had more than 30 fractions of tracking data were combined into one large array. Again, the same Gaussian distribution test was used to quantify the displacement at an all-fraction, all-patient level.

Results

Prostate motion correlation in AP and SI directions

Visually, the AP and SI displacement tends to move together as shown in the first row in Figure 1. The result for the correlation analysis is shown in Table 1. Thirty-nine percent of the fractions show strong correlation in the AP/SI direction, whereas only 12% and 14% of the fractions show strong correlation in RL/AP and RL/SI directions. Moreover, 42% and 44% of the fractions show no correlation in RL/AP and RL/SI directions. The high percentage of correlation in the AP/SI direction (61% medium or strong correlation) is consistent with the longitudinal oblique motion of the prostate, and likely from the effect of respiration on an organ confined within the genitourinary diaphragm with the rectum sitting posterior and the bladder sitting superiorly.

Prostate motion distribution measurement: individual fraction

The results are shown in Table 2. Four examples were selected for presentation as shown in Figure 1.

Case 1 (first column)—This case shows relatively small and stable prostate motion throughout the fraction. The histograms revealed that the displacement in all directions are normally distributed, indicating a random motion in all directions. The 3-dimensional displacement spatial distribution shown in the last row indicates a uniform, small motion in all directions. This is the ideal case where the patient has both constrained physical movement and little internal organ motion.

Case 2 (second column)—This case shows high range of motion with several excursions. In contrast to case 1, the histogram reveals that none of the displacement in any direction is normally distributed. All of them have multiple peaks on their histogram plots. Accordingly, there is no clear pattern of the spatial distribution of the transponder displacement in all directions as shown in the last row.

Case 3 (third column)—This case shows an overall stable motion with a period of excursion toward the end of the treatment. The histogram reveals that the displacement in RL directions shows a nice Gaussian distribution. However, the displacements are not normally distributed in all other directions. As shown in Table 2, 13.6% of all 1024 available fractions had Gaussian distribution in the RL directional the percentage is higher than other directions. The spatial distribution of the transponder displacement shows an elongated pattern in oblique direction, indicating a larger range of motion in AP and SI directions.

Case 4 (fourth column)—This case shows an overall stable but drifting prostate motion. The histogram reveals that the displacement in RL, AP, SI, and oblique directions are not normally distributed where multiple peaks in histogram are observed. However, the displacement in total direction is normally distributed. As shown in the last row, the spatial distribution of the transponder displacement shows an overall uniform distribution in all directions regardless of the non-Gaussian distribution in each individual direction.

In all directions, the non-Gaussian distribution is more common. The RL direction has a higher percentage of Gaussian distribution than other directions.

Prostate motion distribution measurement: total fractions of one patient

The results are shown in Table 3. Three examples were selected for presentation as shown in Figure 2. The number of tracking data is large, and the plot in the first row is downsampled to select every tenth data for presentation purpose.

Patient 1 (first column)—This patient shows overall confined range of prostate motion throughout the treatment. The histograms revealed that the displacements in all directions are normally distributed except the RL direction. The 3-dimensional displacement spatial distribution shown in the last row indicates a uniformly distributed motion in all directions.

Patient 2 (second column)—This patient shows higher range of motion. In contrast to patient 1, the histogram reveals that none of the displacements in any direction is normally distributed. Even though all the histogram is single peaked, the distribution fails to satisfy the normality test based on the shape of the histogram. Accordingly, the spatial distribution of the transponder displacement shows an elongated distribution in oblique direction, indicating a larger range of motion in the AP and SI directions.

Patient 3 (third column)—This patient has large range of motion. Although the histogram revealed the normal distribution in the RL and oblique directions, all the displacements in other directions do not have normal distribution. The spatial distribution of the transponder displacement again shows an elongated distribution in oblique direction.

Again, the non-Gaussian distribution is more common for all directions, and the RL direction has a higher percentage of Gaussian distribution than other directions. A total of 33% and 16.7% of all patients have normally distributed RL and total motion, respectively, and this ratio is approximately twice the percentage for individual fraction for each patient. The accumulative effect from all fractions may explain the increased percentage.

Prostate motion distribution measurement: total fractions from all patients

The results are shown in Figure 3. The number of tracking data is large and the plot in the first row is downsampled to select every hundredth data for presentation purpose. All the tracking data were combined to evaluate whether the Gaussian distribution is a good approximation at a population level. Even through all the histograms have only a single peak (Fig 3b), all of them failed the normality test. The 3-dimensional displacement plot clearly shows an elongated patterned in oblique direction, indicating this trend works at a population level.

Discussion

The intrafraction motion effect is normally modeled and included in the treatment planning as a Gaussian function with random distribution. Bortfeld et al have developed simulation tools and theoretically demonstrated the random motion effect (2, 12). This was also demonstrated using oscillating phantoms experimentally (13–15). Under this assumption, a Gaussian kernel was applied to account for the dose distribution blurring effect caused by organ motion (1, 16). With the 10-Hz real-time tracking data during radiation therapy, we demonstrated that the simple Gaussian-shaped operator may need to be modified for prostate motion because of its specific characteristics. For instance, the higher magnitude of prostate motion is observed in AP and SI directions because of the oblique longitudinal movement of respiration on an organ sitting within the genitourinary diaphragm and confined by the bladder superiorly and the rectum inferiorly. It is also possible that the muscles making up the pelvic floor may limit prostate motion, mainly in the oblique direction. Indeed, this effect is also observed by other researchers previously. Using kV fluoroscopy, Adamson and Wu reported a population mean of 0.1-, 0.5-, and 0.6-mm motion in the RL, AP, and SI axes, respectively (17, 18). Using gold seed fiducial markers, Quan et al observed the mean intra-fraction prostate displacements were −0.03, 0.21, and −0.86 mm in RL, AP, and SI directions, respectively (19). Using Calypso, Willoughby et al reported prostate displacements of 0.9 ± 0.35 mm, 3.61 ± 3.13 mm, and 3.92 ± 4.32 mm in RL, AP, and SI directions, respectively (9). Our results are consistent with the previous clinical reports and suggest that a modified operator should be used to account for the spatial variation of organ motion.

The visual correlation of AP and SI directions has been reported using Calypso electromagnetic tracking system. Kupelian et al reported that a visual review of 1157 fractions of tracking data reveals that the longitudinal (SI direction) and vertical (AP direction) data tend to move together over the tracking session, consistent with the prostate motion being affect by bladder and rectum filling (8). Likewise, we quantified the level of correlation and found about 61% of the tracking data exhibiting strong to medium correlation in AP and SI directions. This conclusion demonstrated that PTV may be reduced in RL direction independently.

Our findings of non-Gaussian prostate motion on an individual and population level are likely a result of the anatomical design of the pelvic floor. The pelvic floor is constituted by the pelvic diaphragm, which is shaped like a funnel, with muscular partitions caused by the levator ani and the coccygeus muscle. The levator ani is further subclassified into the iliococcygeus, pubococcygeus, and puborectalis muscles. All 3 of these muscles run horizontally from an AP direction and are situated laterally to the prostate to form a sling around the prostate (Appendix A, Fig 1). It is possible that because of this sling formation around the prostate motion, the prostate is limited to motion mainly in the AP and SI directions. Laterally, the muscles may limit this motion. The muscular construct of the pelvic floor is one possible explanation of our findings. It is likely that respiration causes motion of the prostate in the SI direction, whereas the anterior deflection of the rectum deflects this motion towards the SP direction. Another explanation may be that the bladder located superiorly and the rectum located posteriorly, both of which are compressible

organs, may also allow for the SI directional movement of the prostate because of respiration to be deflected in an AP direction, especially if the bladder and rectum are full. Hence, this could also cause the prostate to exhibit more of an oblique motion as noted in our findings. Further work by our group is ongoing to assess the impact of respiration and may provide us with further insights about the physiological process that lead to the oblique motion patterns noted in our study.

Conclusion

Prostate motion cannot be accurately described using Gaussian distribution, disregarding the spatial characteristic of the organ motion. The high-frequency, real-time treatment tracking data indicate that the prostate motion is highly correlated in the AP and SI directions, indicating an oblique motion preference. In addition, the spatial distribution of prostate motion is elongated in an oblique direction at the individual fraction level, individual patient level, and population level. Future dosimetric kernel's modeling prostate motion will need to be modified.

Supplementary Material

Refer to Web version on PubMed Central for supplementary material.

References

1. van Herk M. Errors and margins in radiotherapy. Semin Radiat Oncol. 2004; 14:52–64. [PubMed: 14752733]
2. Thomas B, Kimmo J, Michael G, et al. Effects of intra-fraction motion on IMRT dose delivery: Statistical analysis and simulation. Phys Med Biol. 2002; 47:2203. [PubMed: 12164582]
3. Prostate motion during a course of IMRT: The value of daily ultrasound to guide portal localization and correct for random and systematic errors. Radiother Oncol. 2000; 56:S105.
4. Tanyi JA, He T, Summers PA, et al. Assessment of planning target volume margins for intensity-modulated radiotherapy of the prostate gland: Role of daily inter- and intrafraction motion. Int J Radiat Oncol Biol Phys. 2010; 78:1579–1585. [PubMed: 20472357]
5. Webb S. Motion effects in (intensity modulated) radiation therapy: A review. Phys Med Biol. 2006; 51:R403. [PubMed: 16790915]
6. Li HS, Chetty IJ, Enke CA, et al. Dosimetric consequences of intra-fraction prostate motion. Int J Radiat Oncol Biol Phys. 2008; 71:801–812. [PubMed: 18234439]
7. Curtis W, Khan M, Magnelli A, et al. Relationship of imaging frequency and planning margin to account for intrafraction prostate motion: Analysis based on real-time monitoring data. Int J Radiat Oncol Biol Phys. 2013; 85:700–706. [PubMed: 22795802]
8. Kupelian P, Willoughby T, Mahadevan A, et al. Multi-institutional clinical experience with the Calypso System in localization and continuous, real-time monitoring of the prostate gland during external radiotherapy. Int J Radiat Oncol Biol Phys. 2007; 67:1088–1098. [PubMed: 17187940]
9. Willoughby TR, Kupelian PA, Pouliot J, et al. Target localization and real-time tracking using the Calypso 4D localization system in patients with localized prostate cancer. Int J Radiat Oncol Biol Phys. 2006; 65:528–534. [PubMed: 16690435]
10. Noel C, Parikh PJ, Roy M, et al. Prediction of intrafraction prostate motion: Accuracy of pre- and post-treatment imaging and intermittent imaging. Int J Radiat Oncol Biol Phys. 2009; 73:692–698. [PubMed: 18692324]
11. Lilliefors HW. On the Kolmogorov-Smirnov test for the exponential distribution with mean unknown. J Am Stat Assoc. 1969; 64:387–389.

12. Bortfeld T, Jiang SB, Rietzel E. Effects of motion on the total dose distribution. Semin Radiat Oncol. 2004; 14:41–51. [PubMed: 14752732]
13. Steve BJ, Cynthia P, Khaled MAJ, et al. An experimental investigation on intra-fractional organ motion effects in lung IMRT treatments. Phys Med Biol. 2003; 48:1773. [PubMed: 12870582]
14. Li HSCI, Enke CA, Foster RD, et al. The dosimetric consequences of intra-fraction prostate motion in intensity modulation. Int J Radiat Oncol Biol Phys. 2001; 51:214.
15. Langen KM, Chauhan B, Siebers JV, et al. The dosimetric effect of intrafraction prostate motion on step-and-shoot intensity-modulated radiation therapy plans: Magnitude, correlation with motion parameters, and comparison with helical tomotherapy plans. Int J Radiat Oncol Biol Phys. 2012; 84:1220–1225. [PubMed: 22483699]
16. van Herk M, Remeijer P, Lebesque JV. Inclusion of geometric uncertainties in treatment plan evaluation. Int J Radiat Oncol Biol Phys. 2002; 52:1407–1422. [PubMed: 11955756]
17. Adamson J, Wu Q. Prostate intrafraction motion assessed by simultaneous kilovoltage fluoroscopy at megavoltage delivery I: Clinical observations and pattern analysis. Int J Radiat Oncol Biol Phys. 2010; 78:1563–1570. [PubMed: 20579817]
18. Adamson J, Wu Q. Prostate intrafraction motion assessed by simultaneous kV fluoroscopy at MV delivery II: Adaptive strategies. Int J Radiat Oncol Biol Phys. 2010; 78:1323–1330. [PubMed: 20584578]
19. Quon H, Loblaw DA, Cheung PCF, et al. Intra-fraction motion during extreme hypofractionated radiotherapy of the prostate using pre- and post-treatment imaging. Clin Oncol. 2012; 24:640–645.

Summary

The objective of this work is to test the validity of the Gaussian approximation for prostate motion through characterization of its spatial distribution using Calypso 4D nonradioactive electromagnetic tracking system. Our results showed that the prostate motion is highly correlated in the AP and SI directions. In addition, the spatial distribution of prostate motion is elongated in an oblique direction, indicating that the organ motion dosimetric modeling using Gaussian kernel may need to be modified.

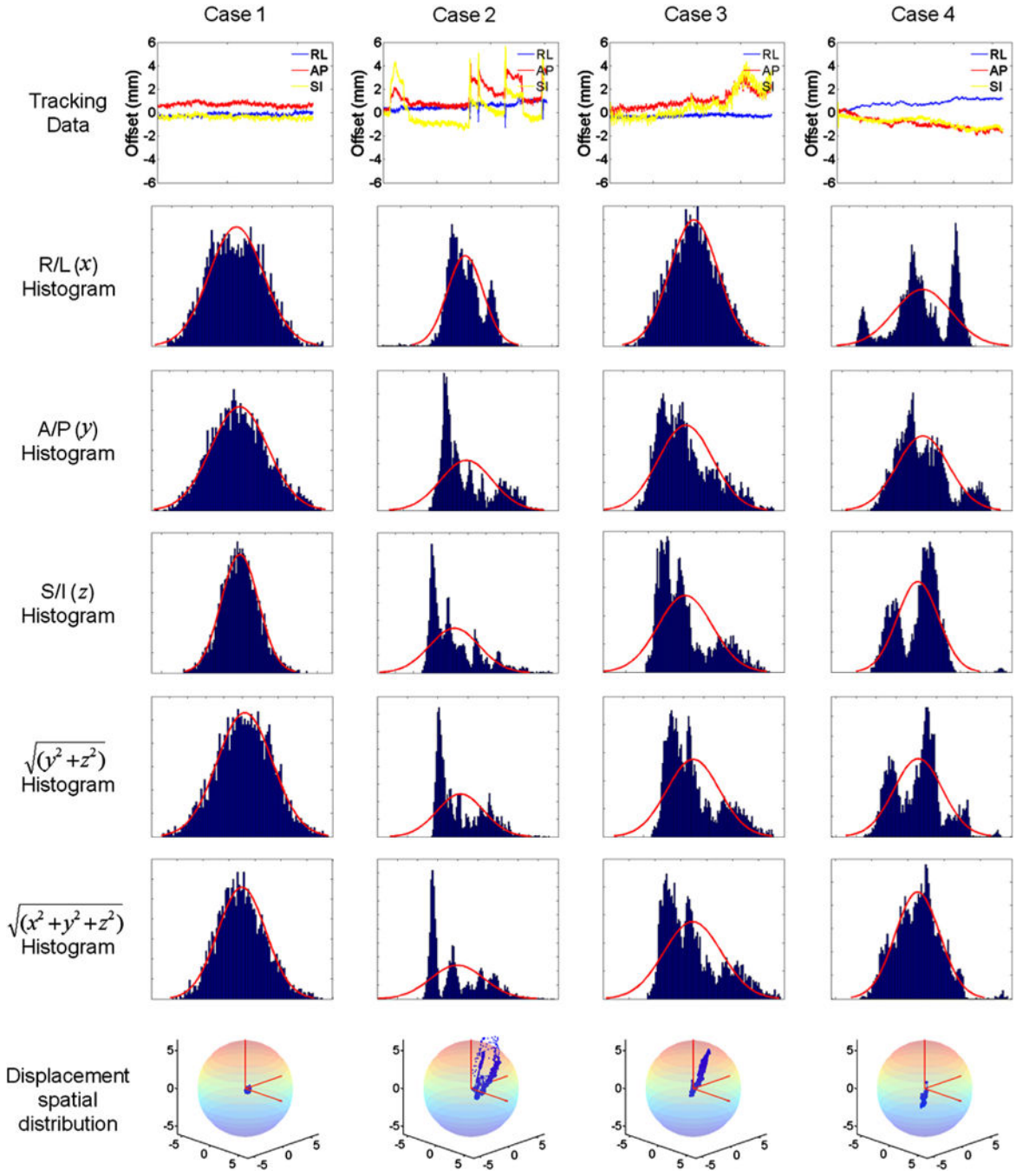

Fig. 1.

Examples of prostate motion distribution analysis for individual fraction. (Row 1) Raw tracking data. (Rows 2–7) Histogram plot for right/left (RL), anteroposterior (AP), superoinferior (SI), oblique, and total directions. (Red line) Gaussian fit of the tracking data overlaid on the histogram. (Row 7) Spatial distribution of the transponder displacement. The upper limit of the x, y, and z axes are set to 6 mm. A color version of this figure can be seen at redournal.org.

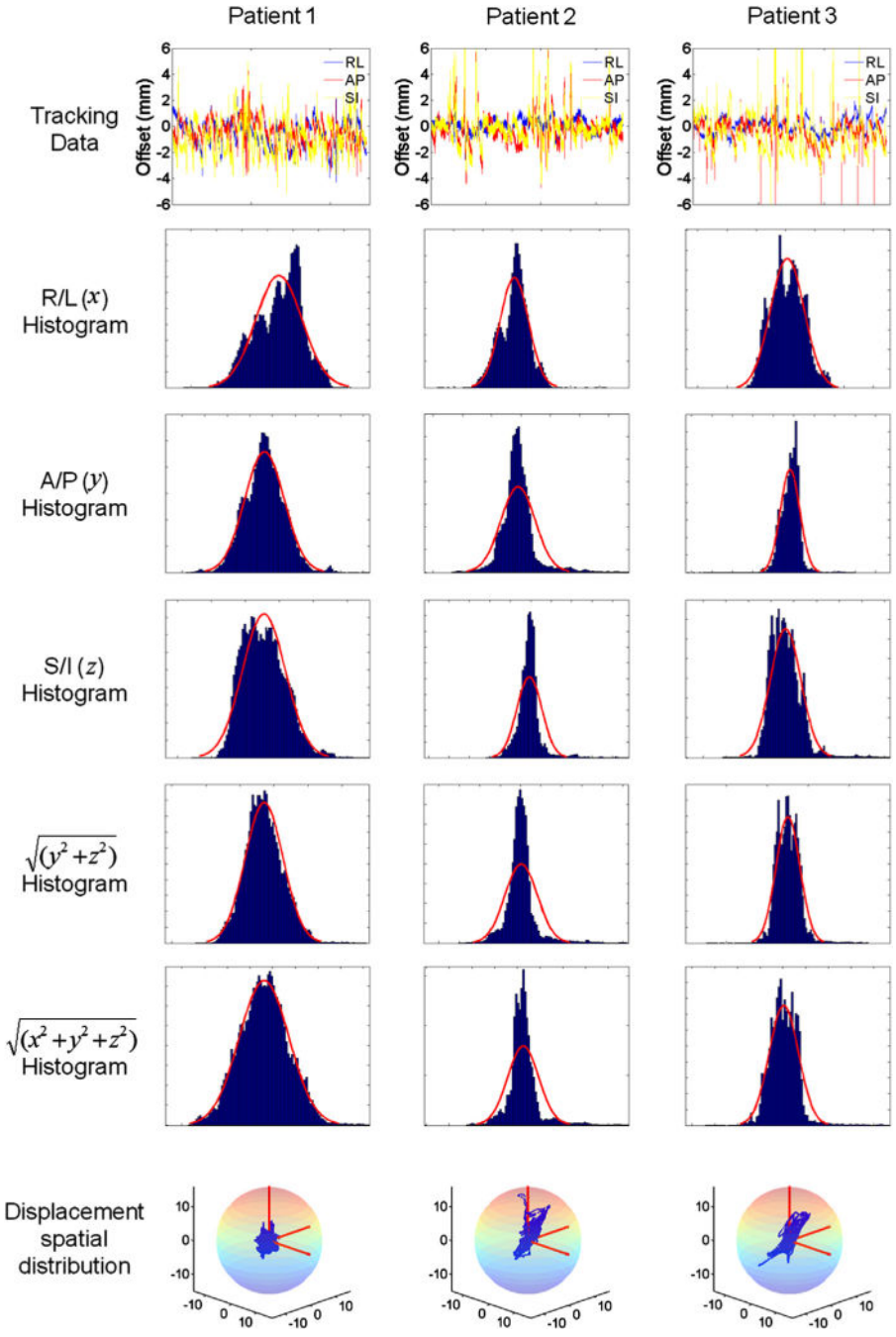

Fig. 2.

Examples of prostate motion distribution analysis for individual patient including all fractions. (Row 1) Downsampled raw tracking data. (Rows 2–7) Histogram plot for right/left (RL), anteroposterior (AP), superoinferior (SI), oblique, and total directions. (Red line) Gaussian fit of the tracking data overlaid on the histogram. (Row 7) Spatial distribution of the transponder displacement. The upper limit of the x, y, and z axes are set to 12 mm. A color version of this figure can be seen at redournal.org.

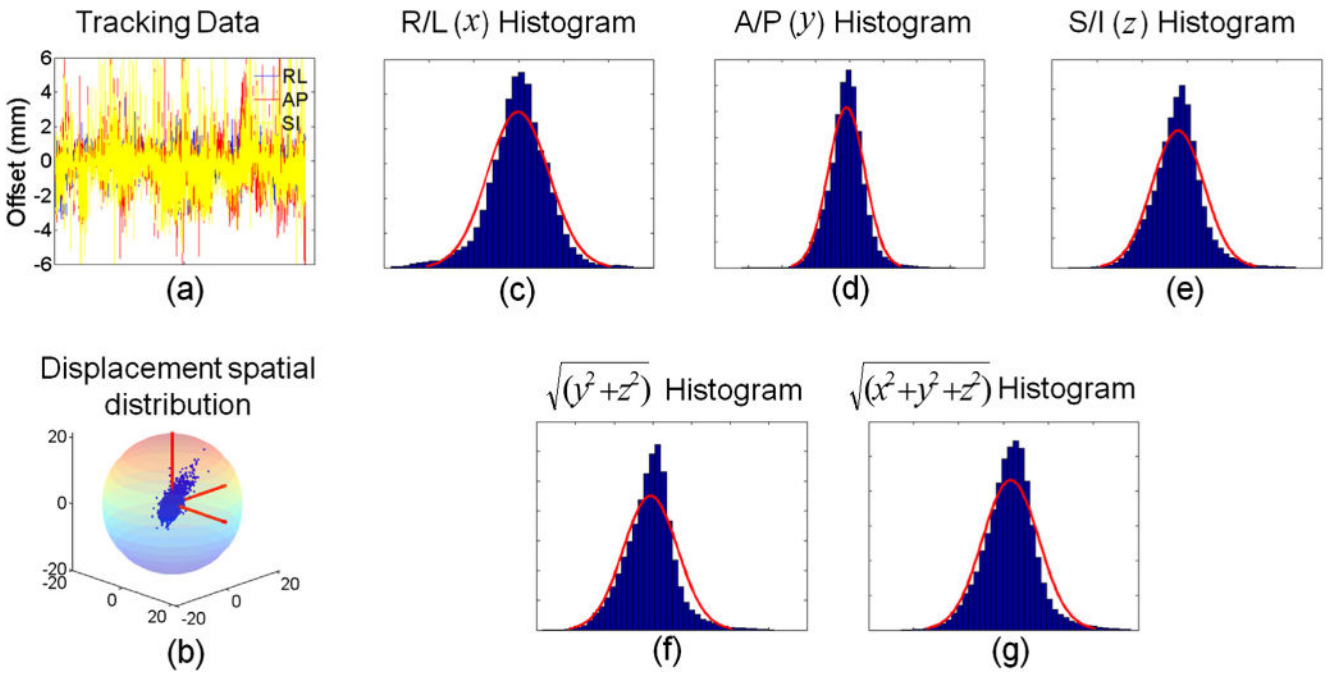

Fig. 3.

Examples of the displacement analysis. (a) Downsampled raw tracking data. (b) Spatial distribution of the transponder displacement. The upper limit of the x, y, and z axes are set to 20 mm. (c–f) Histogram plot for right/left (RL), anteroposterior (AP), superoinferior (SI), oblique, and total directions. (Red line) Gaussian fit of the tracking data overlaid on the histogram. A color version of this figure can be seen at redournal.org.

Table 1

The result for correlation analysis

Correlation	RL/AP	RL/SI	AP/SI
Strong ($R \geq 0.7$)	123 (12%)	141 (14%)	**401 (39%)**
Medium ($0.5 \leq R < 0.7$)	202 (9%)	190 (18%)	231 (22%)
Weak ($0.3 \leq R < 0.5$)	273 (23%)	247 (26%)	173 (17%)
None ($R < 0.3$)	**427 (42%)**	**447 (44%)**	220 (21%)

Abbreviations: AP = anteroposterior; RL = right/left; SI = superoinferior.

The boldface red text emphasizes the strong correlation in AP/SI direction and weak correlation in the RL/AP and RL/SI directions.

Table 2

The result of prostate motion distribution analysis for individual fractions

	RL x axis	AP y axis	SI z axis	Oblique $\sqrt{(x^2+y^2)}$	Total $\sqrt{(x^2+y^2+z^2)}$
Number of fractions with Gaussian distribution	139	77	85	89	89
Percentage of total fractions with Gaussian distribution	13.6	7.5	8.3	8.7	8.7

Abbreviations: AP = anteroposterior; RL = right/left; SI = superoinferior.

A total of 1024 fractions were included in the analysis.

Table 3

The result of prostate motion distribution analysis for individual patient including all fractions

	RL x axis	AP y axis	SI z axis	Oblique $\sqrt{(x^2+y^2)}$	Total $\sqrt{(x^2+y^2+z^2)}$
Number of patients with Gaussian distribution	8	3	2	2	4
Percentage of patients with Gaussian distribution	33	12.5	8.3	8.3	16.7

Abbreviations: AP = anteroposterior; RL = right/left; SI = superoinferior.

A total of 24 patients were included in the analysis.